JJMIE

Volume 20, Number 3, September 2026
ISSN 1995-6665
Pages 447– 462
https://doi.org/10.59038/jjmie/200310
Editor-in-Chief: Prof. Faris M. AL-Oqla

Jordan Journal of Mechanical and Industrial Engineering

Evaluating the Performance of Solid Oxide Fuel Cells with Convergent and Divergent Flow Channel Designs

Arben Avdiu, Bedri Dragusha, Rexhep Selimaj, Drilon Meha*

University of Prishtina, Faculty of Mechanical Engineering, Department of Thermoenergetics and Renewable Energy, Prishtina,10000, Kosovo.

Received 9 Nov 2025 *Accepted 9 May 2026*

Abstract

The development of efficient hydrogen technologies is critical to achieving climate-neutral energy systems. Using a hybrid model that considers both experimental and computational approaches, this research analyzes how different convergent-divergent flow channel configurations can enhance the performance of Solid Oxide Fuel Cells (SOFCs). A baseline SOFC with conventional rectangular channels is compared to 75 different geometric configurations to assess their impact on electrochemical performance. A validated numerical model was created in COMSOL Multiphysics, integrating thermal, chemical, and electrochemical phenomena, with input parameters validated using experimental data from a reference SOFC configuration. Parametric simulations of a counter-flow configuration were carried out to investigate current density distribution, pressure variation, species transport, and water vapor concentration across various flow field designs. The findings show that geometric modifications have a major effect on SOFC performance, particularly at smaller channel dimensions (0.5 mm), with slight effects at larger dimensions (1-1.5 mm). Convergent channel designs enhance performance significantly in the cathode and combined electrode segments, while divergent designs are more effective in the anode and overall cell domains. Test case 39 outscored the baseline configuration by 37.91%, achieving a maximum power density of 0.211 W/cm². These results show that enhanced flow channel geometry can significantly improve SOFC efficiency and serve as a platform for future design advancements in hydrogen-based energy systems.

Keywords: SOFC, flow channel designs, COMSOL, numerical modeling, cell performance.

1. Introduction

It is forecasted that clean production technologies will be essential to sustainable energy systems, particularly in the decarbonization of heavily energy-intensive industries. Fuel cells and other electrochemical technologies facilitate the transformation to low-emission energy conversion and offer flexibility in the power sector. In this regard, hydrogen generated from renewable energy sources offers potential as a long-term decarbonization solution that minimizes additional pressure on natural resources. By using hydrogen as a fuel, fuel cells can efficiently produce both power and heat, with water vapor as the only output, ensuring pollutant-free operation.

Fuel cells are a highly efficient and environmentally friendly energy conversion technology that produces electricity and heat with efficiencies exceeding 80%. They emit minimal CO_2, NO_x, and SO_x (with sulfur removal) and operate quietly without vibration, making them a competitive alternative to traditional power generation systems.

Solid oxide fuel cells (SOFCs) show immense potential for heating and cooling applications in the building sector, as shown in [1]. The efficiency of SOFC can be increased in different ways thus studies focusing on geometric impact have been reviewed and considered as a roadmap to highlight the originality and novelty reported in this research.

Recknagle et al.[2] created a 3D SOFC model to investigate several flow configurations, demonstrating that parallel flow has a more uniform temperature distribution, better thermal stability, and somewhat higher performance than counter and cross-flow designs. A similar study in [3] utilizes a computational model to examine SOFC flow configurations and found that the counter-flow arrangement had lower temperature gradients and yields more hydrogen, making it more suitable for stable and efficient operation. Using 3D numerical modeling, [4] created a shape optimization model for SOFC components and showed that optimized channel configurations improve fuel distribution and performance, especially at high current densities. Furthermore, using finite element analysis, the cell performance of an SOFC with different flow channel geometries, including rectangular, triangular, and trapezoidal was evaluated numerically by [5]. The results obtained by considering a single channel geometry revealed that rectangular channel geometry for SOFC performed better than the triangular and trapezoidal channel designs.

* Corresponding author e-mail: drilon.meha@uni-pr.edu.

Beyond standard SOFC investigations, recent research emphasizes the importance of flow channel design in determining gas dispersion, temperature uniformity, and electrochemical performance. For example, chamfered flow channel designs have shown up to a 15.08% reduction in voltage demand and a 21% reduction in energy usage when compared to conventional geometries, demonstrating the considerable influence of geometric optimization on system performance [6]. Furthermore, unique Y-shaped and converging channel designs have increased hydrogen generation by up to 20.72% and 38%, respectively, while improving temperature uniformity and reducing hotspots [7-8]**.** Furthermore, other studies have shown that advanced system integration solutions, such as exhaust heat recovery and fuel recirculation, can also boost system-level efficiency. For example, innovative SOFC system topologies with ejector-based recirculation and turbocharging processes show significant efficiency increases when operational parameters are optimized [9]. Furthermore, layout optimization based on thermodynamic and heat transfer calculations has shown that appropriate heat integration and afterburner positioning can result in overall system efficiencies of up to 97% [10].

For example, gradient channel anode designs improve fuel distribution and diffusion, contributing to apparent gains in power density [11], whereas asymmetric flow arrangements have been proven to be more effective than symmetric designs due to better local transport properties [12]. Furthermore, innovative channel concepts including loop-flow fields and extended ridge designs can reduce temperature gradients by up to 50% while improving thermal uniformity, resulting in increased durability and efficiency [13-14]. Recent research shows that refined flow field designs, such as radial flow enhancements and oscillatory gas supply techniques, may significantly decrease hotspot intensity while improving thermal performance, even at the expense of greater pressure drop [15-16]. Furthermore, optimization of manifold dimensions and flow field topologies has been found to increase flow uniformity by up to 72% and reduce temperature variations by approximately 30%, emphasizing the significance of integrated geometric design [17]. However, more recent research has shown that other geometries, such as oval or gradient-based channels, can perform better than standard rectangular designs under certain situations by improving mass transfer and lowering polarization losses [11, 18]. Similarly, discrete interconnection designs and optimized rib spacing configurations have shown power density increases greater than 11%, emphasizing the importance of micro-scale geometric optimization [19].

A three-dimensional 3D numerical model is suggested to assess the SOFC performance in [20]. It involves resolving the mass transport, momentum, and energy equations associated with the electrochemical reactions. In comparison to the reference scenario, it is found that the average current density (SOFC performance) increases by 15% when seven triangular obstacles are used.

Danilov and Tade [21] presented a study examining the influence of anode effect of flow field design on cell performance of an internally reformed planar SOFC. The study results showed that the conventional design showed nonlinear velocity, temperature, and local current density distributions, whereas the new design enhanced cell performance by eliminating back mixing and uneven flow distribution. Similar research for planar SOFC operating conditions shows increasing cell performance for high temperature and cathode stochiometric operating regimes [22]. Duhn et al. [23], focuses on parallel flow channels and numerically optimized dimensional flow area geometry of SOFC, using computational fluid analysis. It has been found that the flow in the optimized design has index flow rate value of 0.978. Additionally, the study shows the effect of deviations from the modeling assumption. Li et al.[24] study the optimization of SOFC flow channel width, with the help of the finite element method. The developed mathematical model was compared with the experimental cell performance curve of SOFC. The results obtained when compared numerically and experimentally did not change more than 3%, but they showed a significant dependence of the effect of current density distribution on the variation of gas composition. Numerical resultsindicated that flow channel ribs had a negative effect on electrochemical reactions as they limit the mass transfer. The optimum width ratio for both anode and cathode are reported as 0.5.

Boersma et al. [25] investigated the distribution of flow and pressure along the stack's height, and a two-dimensional simulation model was developed. In the study, where the stack is considered to be a series of hydraulic resistances connected in series and in parallel, counter-flow geometry is proposed for both reactant feeding and waste of products. Output sreveal that when designing the internal manifold, more attention should be paid to the distribution of gas in cathode than the anode side. Li et al. [26] investigate the distribution of flow and pressure along the stack's height, a two-dimensional simulation model was developed. The mathematical model integrated into the Fluent program has been solved numerically for planar SOFC components of the stack, such as manifolds and flow channels and gaskets. Comparative studies have shown that simplifying stack geometry or neglecting multi-physical interactions leads to unreliable results and the necessity of using a real multi-physical calculation tool. Similar general model recommendations are described by Ni [27] and Kee et al. [28]. [27] develops two-dimensional model using the finite volume method and considering laminar flow, conjugate heat transfers and electrochemical reactions, which is found to be compatible with the literature-validated data. The same model can be used to identify complex physical and chemical processes and is therefore suitable for designing and investigating SOFC technologies .On the other side [28] focuses on the numerical analysis of small channel fields in planar SOFCs. A model that predicts flow homogeneity and pressure drop in each channel, focusing on the mass and momentum equation, is proposed. In the study, the problem is formulated with dimensionless variables, and solutions are generalized as two-dimensional groups.

Chemical modifications, nanocomposite membrane development, and electrochemical performance evaluation approaches have been widely reported in proton exchange membrane (PEM) fuel cells, where membrane composition and structure heavily influence cell voltage-current behavior and overall performance [29].

Nishida et al. [30] developed a CFD model for large SOFC stacks, demonstrating that the input flow distribution has a significant impact on temperature and performance, and that precise coupling of transport and electrochemical phenomena is necessary for reliable design and optimization.

1.1. State of the art

Despite significant advances in SOFC research, a thorough examination of the literature indicates a number of remaining challenges that limit further performance enhancement and application. Existing research primarily treats flow distribution, heat management, and electrochemical behavior as separate problems, resulting in a scarcity of integrated optimization frameworks capable of capturing their substantial interdependence. In particular, the importance of convergent and divergent channel geometries is poorly understood, particularly regarding coupled transport processes that govern mass, heat, and charge movement inside the cell. Furthermore, while more advanced computational models have been widely developed, experimental validation under realistic operating environments remain limited, thereby lowering credibility in their forecasting capability.

This gap is heightened by the lack of systematic investigation into modified rectangular channel designs, despite their industrial relevance and steady baseline performance when compared to other geometries. Although counter-flow configurations have been shown to improve current density uniformity and thermal stability, and compact multi-channel stacks show promising power density improvements [31-32], the link between cell-level geometric design and system-level performance optimization is still weak.

To address these limitations, the current study presents a combined experimental and multi-physics numerical technique for systematically evaluating the effect of convergent and divergent flow channel designs on SOFC performance. Unlike prior efforts that focused on isolated geometric adjustments, this study uses rectangular channel geometry as a reference instance and applies different geometric variations to improve flow uniformity and thermal behavior. The analysis considers both thermodynamic (flow distribution, temperature fields, and pressure losses) and electrochemical (current density, voltage, and power density) responses, providing a comprehensive evaluation of performance.

The numerical model, created in COMSOL Multiphysics, is tested against experimental data collected from a laboratory-scale SOFC system, increasing the reliability of the results. Furthermore, a counter-flow configuration is selected based on its reported advantages in the literature, and multiple test scenarios are run to determine the impact of reconfiguration anode and cathode channel configurations on the overall cell efficiency. The research's integrated methodology aims to fill the gap between numerical modeling and experimental validation, thereby contributing to the design of high-performance rectangular SOFC systems.

2. MATERIAL AND METHODS

A mathematical model was used in COMSOL Multiphysics to research the novel design of different channels flow geometries on thermodynamic aspects such as fuel (Hydrogen) flow, air flow, temperature distribution, and pressure losses as well as electrical indicators such as power density curve, current and voltage. Experimental investigations were performed in the Laboratory in Niğde Ömer Halisdemir University and compared with the numerical model developed in COMSOL for the rectangular cell stack (base case). The counter flow SOFC is considered due to greater performance shown as compared with other flow configuration streams, and several scenarios through test cases numerically have been employed to investigate the impact of convergent and divergent channel flow designs especially in power density curve behavior and increasing cell performance rate. Scenarios consider the modification of rectangular model geometries while simultaneously re-arranging convergent and divergent anode and cathode flow distribution geometries.

2.1. Experimental setup investigations and analysis

For validation purposes, anexperimental model was developed in Niğde Ömer Halisdemir University[1], and supported from Lentatek Aerospace and Technology Inc with laboratory infrastructure and material. The graphical ilustration of experimental setup is shown in Fig. 1. An electrolyte supported membrane including an active area of 16 cm^2 was used. While 300 standard cubic centimeters per minute (SCCM) of hydrogen was fed to the anode region through flow channels, 900 SCCM of oxygen was sent to the cathode region. Considering that only single flow channel is included in the numerical model, the amount of gases fed to the anode and cathode is divided into thirteen and defined as a constant value for the single flow channel. Similar to the experimental study, the flow configuration of gases modeled in COMSOL is counter-flow. In cell tests; test station, impedance measuring device, electronic oven, air compressor, gas tanks and computers were used.

Figure 1. Schematic view of the experimental lab and the devices (Own illustration)

Materials of SOFC significantly impact on the mechanical and economic aspects of design and operation, hence a variety of them can be found in literature [33-36]. In this study, zirconium oxide stabilized with yttrium oxide electrolyte (YSZ) supported SOFC an active area in a single unit cell of 16 cm^2 was tested at 750 °C, and its performance was measured. The channel length of a single cell with counter-flow configuration is 40 mm, and channel depth, rib width and channel width are 1.5 mm. Performance of a single cell results were obtained under hydrogen (300mL / min) and air (900mL / min) at 750 °C. Hydrogen and

[1]Prof. Dr. T. Nejat Veziroglu Clean Energy Application and Research Center.

airflow rates are defined as 1/13 of the experimental study since there are 13 channels in the experimental setup. Models were isothermally solved at 750 °C.

2.2. Modeling and Parametric Analysis

The numerical model was solved with the help of the Batteries & Fuel Cells module in the commercial COMSOL Multiphysics® program. Ohm's law applied to electronic and ionic charge distribution, charge transfer behavior described by the Butler-Volmer, distribution of gas flow within channels (modeled using Navier-Stokes equations), distribution of flow within porous electrodes (modeled using the Brinkman equation) characterizing the events occurring during SOFC operation (Ohm's law). Electrochemistry and flow analyses including mass balance (Maxwell-Stefan diffusion) gas channels and porous electrodes were simulated.

A detailed description of mathematical equations is provided in 2.3 subsections of mathematical modeling. Analysis performed under steady-state and isothermal conditions were performed on a Dell brand work station. Our numerical simulations were performed for voltage values between 0.1 and 1 V, with the corresponding model parameters listed in Table 1.

Table 1. Model input parameters

Parameter	Value
Operating Temperature [ºC]	750
Working Pressure [atm]	1
Viscosity of Air [Pa s]	3x10-5
Permeability of Anode[m^2]	10-10
Permeability of Cathode [m^2]	10-10
Specific Anode Surface Area [1/m]	109
Specific Cathode Surface Area [1/m]	109
Ionic conductivity of the anode[S/m]	1
Cathode Ionic Conductivity [S/m]	1000
Cathode Ionic Conductivity [S/m]	1
Cathode Electronic Conductivity [S/m]	1000
Electrolyte Ionic Conductivity [S/m]	5
Interconnector Conductivity [S/m]	500
Reference Diffusion[m^2/s]	3.16x10-8
Hydrogen Kinetic Volume [m^3/mol]	$6x10^{-6}$
Oxygen Kinetic Volume[m^3/mol]	$16.9x10^{-6}$
Nitrogen Kinetic Volume [m^3/mol]	$17.9x10^{-6}$
Water Kinetic Volume [m^3/mol]	$12.7x10^{-6}$
Porosity	0.35
Cell Operating Voltage [V]	0.1-1
Channel Width of Gas Flow [mm]	1.5
Channel Height Gas Flow[mm]	1.5
Thickness of Anode [mm]	0.03
Thickness of Cathode [mm]	0.03
Thickness of Electrolyte [mm]	0.15
Length of Flow Channel [mm]	40
Hydrogen inlet mass ratio [%]	97
Oxygen inlet mass ratio [%]	23.14

The rectangular channel geometry of the SOFC, which has been mathematically modeled and analyzed numerically, is given in Figure 2. The base modeling and scenario analysis were performed with the help of COMSOL Multiphysics® program on a single cell containing flow channels of the cathode and anode, along with the membrane electrode assembly. The SOFC membrane electrode group consists of a mixture of NiO/YSZ (50%-50% by mass), anode of NiO/YSZ (50%-50% by mass), and LSM/YSZ (50%-50% by mass) in equal proportions by mass. Electrolyte material is YSZ.

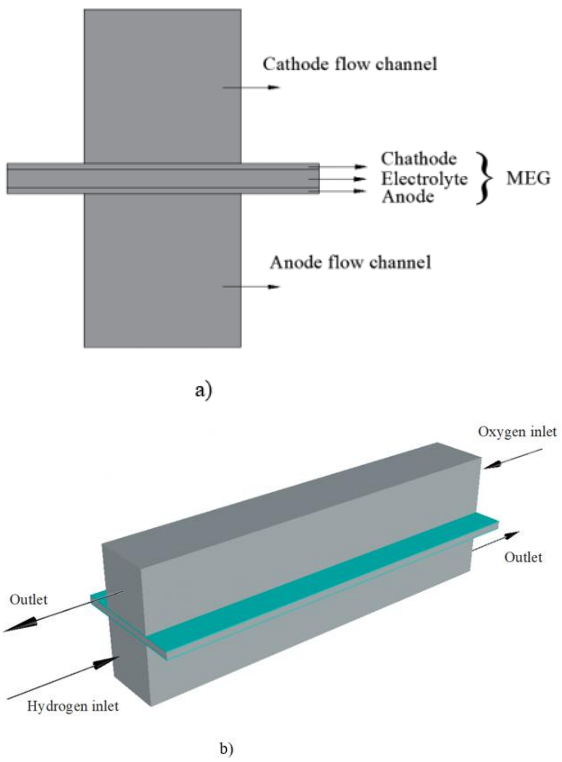

Figure 2. Cross-section (a) and 3D (b) view of the SOFC reference model

The dimensions of the base case design are given in Figure 3.

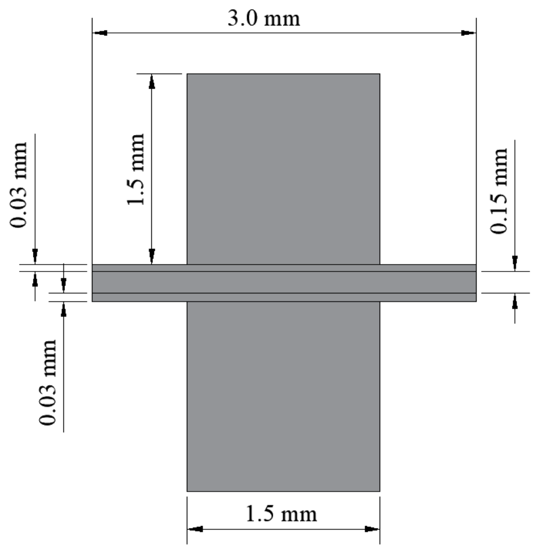

Figure 3. Dimensions of the investigated SOFC base case model

In the following section, the validation methodology is described, including the meshing approach and parameter definition.

2.2.1. Boundary Conditions and Study State Model Adaptation

The mass ratio applied to both the anode and cathode inlets were entered as constant and the pressure at the outlets was adjusted to atmospheric pressure. Gases are considered as ideal gases. Computational studies were conducted ata constant temperature of 750 ºC. Walls are considered insulated and a no-slip condition is applied. The analysis was performed in a steady state. The numerical simulations were carried out using a stationary solver in COMSOL Multiphysics. The governing equations were solved simultaneously using a fully coupled technique, resulting in substantial coupling between the electrochemical, thermal, and flow fields. The linear system was solved with the PARDISO direct solver, which is resilient and efficient for large-scale multiphysics problems.

The convergence requirements were established as a relative tolerance of 1×10^{-12}, a tolerance factor of 1, and a maximum of 100 nonlinear iterations. To improve convergence stability, pseudo-time stepping was used as a stabilization and acceleration strategy, with a maximum iteration of 200 and a relative tolerance of 0.01. These solver configurations were chosen to ensure numerical stability, precision, and dependable convergence of the coupled system of equations under the operating conditions studied.

2.2.2. Base case model geometry mesh

The model geometry consists of one membrane electrolyte group (MEG) and flow paths for both the anode and cathode, in conjunction with the experimental work employed to validate the mathematical model. The view of the meshed structure of the reference case model is given in Figure 4. While triangular mesh was applied to gas channels, a structural mesh was applied to other sections. Since the electrochemical processes occurred mostly at the interfaces between the anode and electrolyte and the cathode and electrolyte, a finer mesh is applied to the areas of the anode and cathode near the electrolyte. The numerical simulations were performed using COMSOL Multiphysics® v6.0 to solve the fully coupled nonlinear system of governing equations. A mesh predefined custom independence study was conducted for the SOFC using grids containing 0.17955×10^6 elements. The mesh statistics and sizes are summarized in table 2.

Table 2. Mesh statistics and size

Description	Value	Description	Value
Status	Complete mesh	Maximum element size	0.004
Mesh vertices	12320	Minimum element size	7.2E-4
Prisms	14499	Curvature factor	0.6
Hexahedra	3456	Resolution of narrow regions	0.5
Number of elements	17955	Maximum element growth rate	1.5
Minimum element quality	0.6433		
Average element quality	0.9198		
Element volume ratio	0.032049		
Mesh volume	9.36E-8 m³		

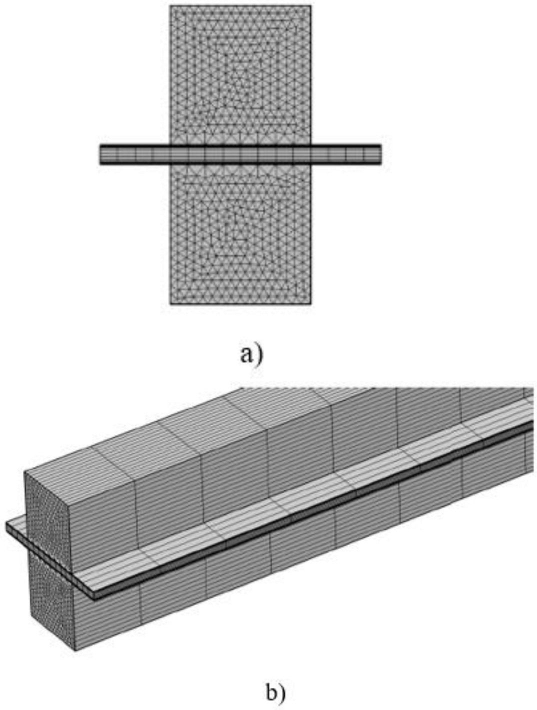

Figure 4. Cross-section (a), three-dimensional (b) mesh view of the SOFC base case model

2.3. Mathematical modeling

Although the structure of fuel cells is relatively simple, its operation is extremely difficult to model because it involves many different physics. The inputs used for accurate fuel cell modeling, contain a large number of coefficients to be determined, thus they must take into account the flow characteristics, heat and mass transfer as well as electrochemical processes. The operating principle of fuel cells can be defined by conservation equations that incorporate physics integrally. The mathematical model must take into account the inhomogeneous character of the fuel cell structure. Therefore, conservation equations should typically be written and resolved separately for SOFC components such as flow channels, electrodes, electrolytes, and interconnections. A mathematical model including this physics is given below.

2.3.1. Momentum Equation

Fluid pressure and velocity variations in spatial regions flow in the anode and cathode flow channels can be given by Navier-Stokes equations:

$$\rho\frac{\partial\mathbf{u}}{\partial t}+\rho\mathbf{u}\cdot\nabla\mathbf{u}= -\nabla p+\nabla\left[\mu(\nabla\mathbf{u}+(\nabla\mathbf{u})^T)-\frac{2}{3}\mu(\nabla\cdot\mathbf{u})\mathbf{I}\right]+\mathbf{F} \tag{1}$$

The Brinkman equation for porous media flow, such as anode and cathode, is given below as a combination of momentum and continuity equations, including viscous

$$\frac{\rho}{\varepsilon_p}[\frac{\partial \mathbf{u}}{\partial t}+(u\cdot\nabla)\frac{\mathbf{u}}{\varepsilon_p}]= -\nabla p+\nabla\cdot\{\frac{1}{\varepsilon_p}[\mu(\nabla\mathbf{u}+(\nabla\mathbf{u})^T)-\frac{2}{3}\mu(\nabla\cdot\mathbf{u})\mathbf{I}]\}-[k^{-1}\mu+\frac{Q_{br}}{\varepsilon_p^2}]\mathbf{u}+\mathbf{F} \quad (2)$$

$$\frac{\partial}{\partial t}(\varepsilon_p\rho)+\nabla\cdot(\rho\mathbf{u})=Q_{br} \quad (3)$$

In these equations, $\varepsilon_p$is porosity, k is permeability, ρ is the density of the gas mixture, and is given as follow:

$$\rho=\sum_{j=1}^{N}\rho_j\, c_j \quad (4)$$

Using the ideal gas law, the density of each substance is evaluated.

2.3.2. Mass conservation

Mass diffusion and transport are defined by Maxwell-Stefan equation:

$$\nabla\cdot\mathbf{j}_i+\rho(\mathbf{u}\cdot\nabla)\omega_i=R_i \quad (5)$$

$$N_i\mathbf{j}_i+\rho\mathbf{u}\omega_i \quad (6)$$

In this numerical framework the mass conservation of each chemical species *i* is described using a species transport equation.

Diffusion flux of spices*i* is given as follow:

$$\mathbf{j}_i=(\rho D_i^m\nabla\omega_i+\rho\omega_i D_i^m\frac{\nabla M_n}{M_n}- \rho\omega_i\sum_k\frac{\nabla M_i}{M_n}D_k^m\nabla x_k D_i^T\frac{\nabla T}{T}) \quad (\quad (7)$$

Where ρ and u represent the density of gas mixture and the bulk flow velocity, respectively ω_I represents the mass friction of species *i* and j_i corresponds to mass flux relative to mass average velocity. R*i* represents the net rate of production or consumption of species *i* due to chemical reactions.

Where D and M represent the diffusion coefficient and molar mass. x donotes mole friction and T presents the temperature. The thermal diffusion coefficient is given as:

$$D_i^T=\frac{1-\omega_i}{\sum_{k\neq 1}\frac{x_k}{D_k}} \quad (8)$$

The average molar mass can be defined as follows:

$$M_n=(\sum_i(\frac{\omega_i}{M_i})^{-1} \quad (9)$$

2.3.3. Electrochemistry and charge transport equations

Butler-Volmer equation is used to express the current–voltage relations of the electrochemical processes:

$$i=i_o[C_R\exp(\frac{\alpha_a nF\eta}{RT})-C_o\exp(\frac{\alpha_c nF\eta}{RT})] \quad (10)$$

where: i_o –stands for the exchange current density, n -is the number of electrons taking part in each electrode reaction, α_a and α_c - Correspond to the charge transfer coefficients for the anode and cathode, respectively, and η - represents the overpotential, determined from the balance of electrode potentials:

$$\eta_a=\phi_{elec}-\phi_{ion}-E_{eq\_a} \quad (11)$$

$$\eta_c=\phi_{elec}-\phi_{ion}-E_{eq\_c} \quad (12)$$

2.3.4. Heat transfer

Temperature is a critical factor that may significantly influence SOFC performance.

To account for this, the model includes thermal transfer methods as conduction, convection, and electrochemical heating. These processes specify the heat sources within the domain and at its limits, taking into account both irreversible heat generation (such as Joule heating and activation losses) and reversible heat. The energy conservation equation that governs the thermal behavior of the cell is written as follows:

$$\rho C_p(\mathbf{u}\nabla T)=\nabla(k\nabla T)+Q \quad (13)$$

where ρ density, c_p heat capacity, and k thermal conductivity are material properties, **u** is the velocity field and Q represents heat sources/ sinks.

2.4. Modeling the scenario of geometrical flow channel designs

In order to understand the optimum channel geometry by examining the convergent-divergent channel designs, 75 different convergent-divergent channel designs were determined, geometries were created, and the necessary analyses were carried out using a verified mathematical model. 75 different situations studied within the scope of the thesis are given in Table 3 and Table 4. While creating the aforementioned conditions, the depths of anode and cathode channel were reduced up to 20% in the convergent channel design, and increased at different rates, starting from 20% in the design of the diverging channel, depending on the width ofthe channel and rib.

Table 3. Convergent channel designs

Test case	Width of the channel [mm]	Width of rib [mm]	Depth of the channel [mm]		Depth of the channel [mm]	
			Anode inlet	Anode outlet	Cathode inlet	Cathode outlet
Base case	1.5	1.5	1.5	1.5	1.5	1.5
Case 2	1.5	1.5	1.5	1.2	1.5	1.5
Case 3	1.5	1.5	1.5	0.9	1.5	1.5
Case 4	1.5	1.5	1.5	0.6	1.5	1.5
Case 5	1.5	1.5	1.5	0.3	1.5	1.5
Case 6	1.5	1.5	1.5	1.5	1.5	1.2
Case 7	1.5	1.5	1.5	1.5	1.5	0.9
Case 8	1.5	1.5	1.5	1.5	1.5	0.6
Case 9	1.5	1.5	1.5	1.5	1.5	0.3
Case 10	1.5	1.5	1.5	1.2	1.5	1.2
Case 11	1.5	1.5	1.5	0.9	1.5	0.9
Case 12	1.5	1.5	1.5	0.6	1.5	0.6
Case 13	1.5	1.5	1.5	0.3	1.5	0.3
Case 14	1	1	1	1	1	1
Case 15	1	1	1	0.8	1	1
Case 16	1	1	1	0.6	1	1
Case 17	1	1	1	0.4	1	1
Case 18	1	1	1	0.2	1	1
Case 19	1	1	1	1	1	0.8
Case 20	1	1	1	1	1	0.6
Case 21	1	1	1	1	1	0.4
Case 22	1	1	1	1	1	0.2
Case 23	1	1	1	0.8	1	0.8
Case 24	1	1	1	0.6	1	0.6
Case 25	1	1	1	0.4	1	0.4
Case 26	1	1	1	0.2	1	0.2
Case 27	0.5	0.5	0.5	0.5	0.5	0.5
Case 28	0.5	0.5	0.5	0.4	0.5	0.5
Case 29	0.5	0.5	0.5	0.3	0.5	0.5
Case 30	0.5	0.5	0.5	0.2	0.5	0.5
Case 31	0.5	0.5	0.5	0.1	0.5	0.5
Case 32	0.5	0.5	0.5	0.5	0.5	0.4
Case 33	0.5	0.5	0.5	0.5	0.5	0.3
Case 34	0.5	0.5	0.5	0.5	0.5	0.2
Case 35	0.5	0.5	0.5	0.5	0.5	0.1
Case 36	0.5	0.5	0.5	0.4	0.5	0.4
Case 37	0.5	0.5	0.5	0.3	0.5	0.3
Case 38	0.5	0.5	0.5	0.2	0.5	0.2
Case 39	0.5	0.5	0.5	0.1	0.5	0.1

Table 4. Divergent channel designs

Test case	Width of the channel [mm]	Width of rib [mm]	Depth of the channel [mm]		Depth of the channel [mm]	
			Anode inlet	Anode outlet	Cathode inlet	Cathode outlet
Base case	1.5	1.5	1.5	1.5	1.5	1.5
Case 40	15	1.5	1.2	1.5	1.5	1.5
Case 41	1.5	1.5	0.9	1.5	1.5	1.5
Case 42	1.5	1.5	0.6	1.5	1.5	1.5
Case 43	1.5	1.5	0.3	1.5	1.5	1.5
Case 44	1.5	1.5	1.5	1.5	1.2	1.5
Case 45	1.5	1.5	1.5	1.5	0.9	1.5
Case 46	1.5	1.5	1.5	1.5	0.6	1.5
Case 47	1.5	1.5	1.5	1.5	0.3	1.5
Case 48	1.5	1.5	1.2	1.5	1.2	1.5
Case 49	1.5	1.5	0.9	1.5	0.9	1.5
Case 50	1.5	1.5	0.6	1.5	0.6	1.5
Case 51	1.5	1.5	0.3	1.5	0.3	1.5
Case 14	1	1	1	1	1	1
Case 52	1	1	0.8	1	1	1
Case 53	1	1	0.6	1	1	1
Case 54	1	1	0.4	1	1	1
Case 55	1	1	0.2	1	1	1
Case 56	1	1	1	1	0.8	1
Case 57	1	1	1	1	0.6	1
Case 58	1	1	1	1	0.4	1
Case 59	1	1	1	1	0.2	1
Case 60	1	1	0.8	1	0.8	1
Case 61	1	1	0.6	1	0.6	1
Case 62	1	1	0.4	1	0.4	1
Case 63	1	1	0.2	1	0.2	1
Case 27	0.5	0.5	0.5	0.5	0.5	0.5
Case 64	0.5	0.5	0.4	0.5	0.5	0.5
Case 65	0.5	0.5	0.3	0.5	0.5	0.5
Case 66	0.5	0.5	0.2	0.5	0.5	0.5
Case 67	0.5	0.5	0.1	0.5	0.5	0.5
Case 68	0.5	0.5	0.5	0.5	0.4	0.5
Case 69	0.5	0.5	0.5	0.5	0.3	0.5
Case 70	0.5	0.5	0.5	0.5	0.2	0.5
Case 71	0.5	0.5	0.5	0.5	0.1	0.5
Case 72	0.5	0.5	0.4	0.5	0.4	0.5
Case 73	0.5	0.5	0.3	0.5	0.3	0.5
Case 74	0.5	0.5	0.2	0.5	0.2	0.5
Case 75	0.5	0.5	0.1	0.5	0.1	0.5

The results and discussion of the base case model, experimental validation, and scenario analysis are provided in the section below.

3. RESULTS AND DISCUSSION

The following shows the results of modeling and experimental setup investigations for the base case model yielded through model validation assessment as well as additional scenarios that include respective changes in flow distribution channel geometries from both anode and cathode regions.

3.1. Validation of the base case numerical and experimental model

Several cell performance indicators, such as voltage, current density, and power density curves, were used to validate the base model through comparison of numerical and experimental results. The SOFC performance indicators are presented graphically in Figure 5. The results show good agreement between computational calculations and experimental measurements for the selected numerical parameters. In numerical analysis, maximum power densityof 0.1526 W/cm^2 was achieved at an operating voltage of 0.5 V, confirming good agreement with input data from experimental observations.

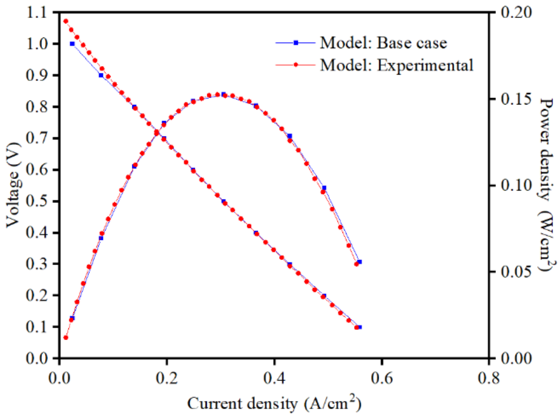

Figure 5. Comparison of cell performance curves from simulations and experiments.

A simultaneous approach was used to find the optimal values of parameters depicted in Table 4 that were needed for model validation in the numerical base case model. The constraints of parameters included variations from $i_{0,anode}$=0.02-0.07; $\alpha_{a,anaode}$=0.05-1; $\alpha_{c,anode}$=1-1.5; $i_{0,cathode}$ =0.01-0.05; $\alpha_{a,cathode}$=3-3.5; $\alpha_{a,cathode}$=0.5-1. A combination mix of parameters shown in Table 5 that showed the best agreement with experimental data is used and harmonized in the numerical modeling of the rectangular SOFC model and other test cases.

Table 5. Optimized combined mix of parameters used in numerical modeling

Parameter	Value	Unit
$i_{0,}$ anode	0.05	[A/m^2]
$\alpha_{a,}$ anode	0.5	-
$\alpha_{c,}$ anode	1.22	-
$i_{0,}$ cathode	0.04	[A/m^2]
$\alpha_{a,}$ cathode	3.01	-
$\alpha_{c,}$ cathode	0.5	-

Once the base case model was validated the next step included the numerical analysis of novel flow channel designs and their impact on the overall investigated assessments of new SOFC performance designs.

3.2. Scenario numerical modeling of novel convergent and divergent channel flow geometries

Channel flow geometries were numerically modeled in COMSOL multiphysics for both convergent and divergent hydrogen and air flow distributions. The modeling results are evaluated through power density, voltage and current curves for all assessed test cases and only cases that have shown greater cell performance changes to the base case model are further discussed and presented graphically, whereas other cases did not show any significant variation in the performance assessment (those presented in test case tables 3 and 4) therefore, they are excluded from further investigation.

3.2.1. Convergent channel design

In convergent channel designs, the case in which the channel width, rib width, and channel depths are each 1.5 (mm) is considered the base case. In addition, not only the effect of convergence (channel depth variation illustrated in Fig. 6) but also the influence of other channel geometrical parameters was evaluated. In the convergent channel configurations: the channel and rib widths, as well as the channel depths, at the anode and cathode gas inlets were kept constant, while different geometries were generated by varying the ratio of the channel depth at the gas outlets to the inlet channel depth (a/b) between 1 and 5 (Figure 6).

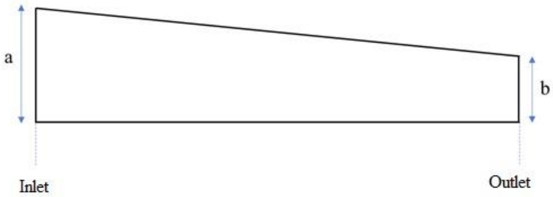

Figure 6. Convergent channel design

Figure 7 shows the role of a/b ratio in the convergent **anode flow channel** on cell performance for different flow geometries. It is observed that variations in the a/b ratio, for geometries where the rib width, channel depth, and channel width are designed as 1.5 (mm), 1.0(mm), and 0.5 (mm) do not have a significant impact on the overall performance. Compared to the base case, the variations reflected in test cases 15-18 and 28-31, show a notable increase in cell performance, as observed by the power density curves. In contrast, test cases 2-5 do not exhibit any improvement in performance relative to the base case. Furthermore, the configurations shown in Fig 7c demonstrate higher performance enhancement compared to the cases presented in Fig 7a and 7b respectively.

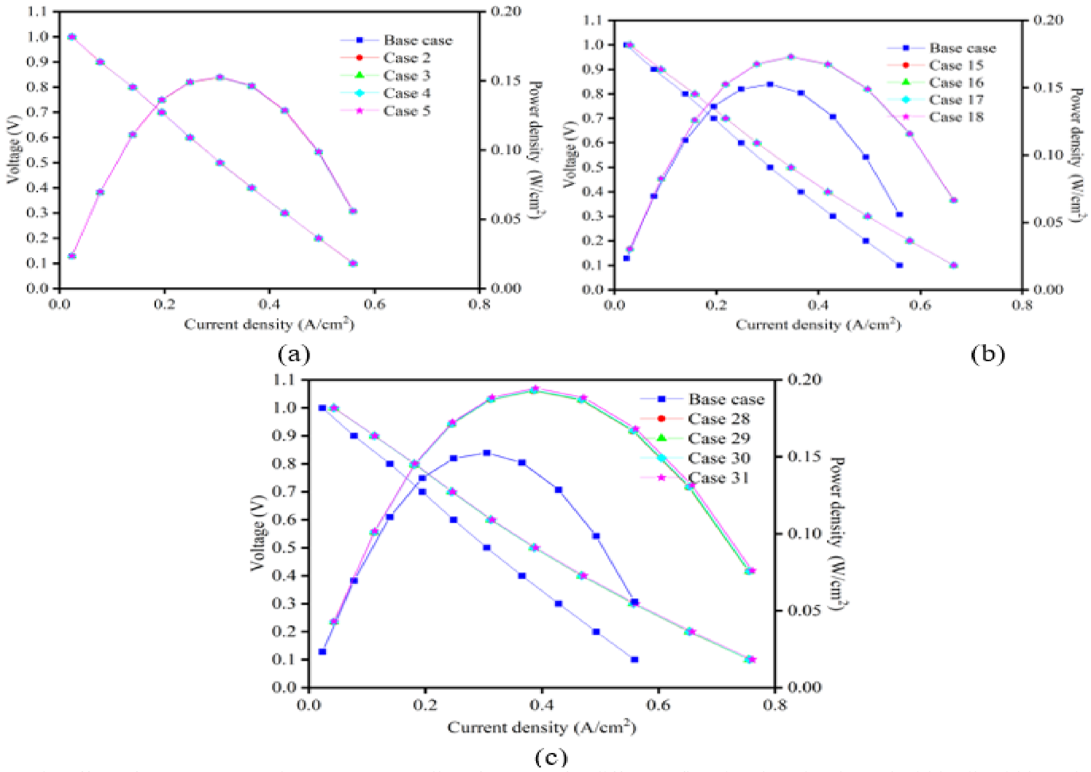

Figure 7. The effect of convergent anode geometry on cell performance for different a/b ratio when the channel width, rib width, and channel depth are 1.5 mm (a), 1 mm (b), and 0.5 mm (c)

The effect of a/b ratios in the **convergent cathode flow channel** on the cell performance for different flow geometriesis elicited in Figure 8. It is shown that changes in the a/b ratio do not impact the performance when the rib width, channel depth, and channel width are designed as 1.5 (mm) and 1.0(mm)(Fig. 8a). However, obvious change in cell performance is observed when these parameters are reduced to 0.5 (mm) (Fig.8b and 8c). For this cathode geometry, cell performance improves with increasing a/b ratio. This behavior is attributed to a more homogeneous mass distribution resulting from the reduced cross-sectional area, despite reactant consumption along the electrochemical reaction path. Similarly, test cases 14, and 20-22 show improved performance compared to the base case, while other convergent cathode channel cases do not exhibit significant changes. Among the cases presented in Figures 8 a, 8b and 8c, test case demonstrate the highest performance improvement compared to other cases.

Figure 9 shows theflow channel configurationswith asimilar a/b ratios for both anode and cathode channels on cell performance. It is observed that variations in the a/b ratio do not significantly affect cell performance when the channel depth, rib width, and channel width are 1.5 (mm) and 1.0(mm)(Fig. 9a). In cases where channel depth, rib width, and channel width were 0.5 (mm), cell performance improves with increasing a/b ratio (Figs. 9b and 9c). Although reactant consumption occurs along at the end of the electrochemical reactions, this improvement is attributed to a more homogeneous gas distribution resulting from the reduced cross-sectional area. Among the convergent channel configurations considered, test case 39 demonstrated the highest performance, achieving a power density of 0.211 W/cm^2. In comparison, the base case, aligned with experimental conditions, yielded a maximum power density of 0.153 W/cm^2.

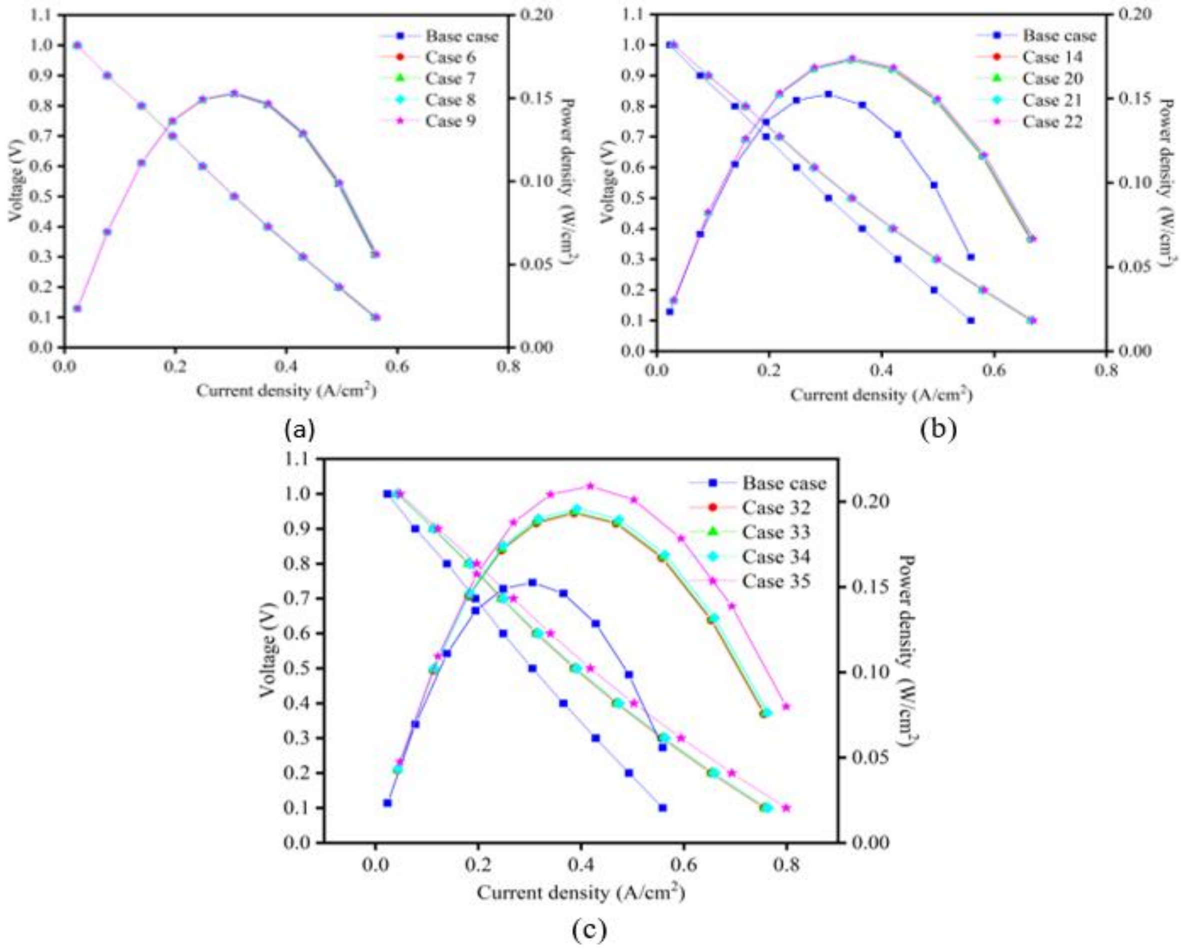

Figure 8. Effect of convergent cathode geometry on cell performance for different a/b ratio when channel depth, rib width, and channel width are 1.5 (mm) (a), 1.0 (mm) (b), and 0.5 (mm) (c)

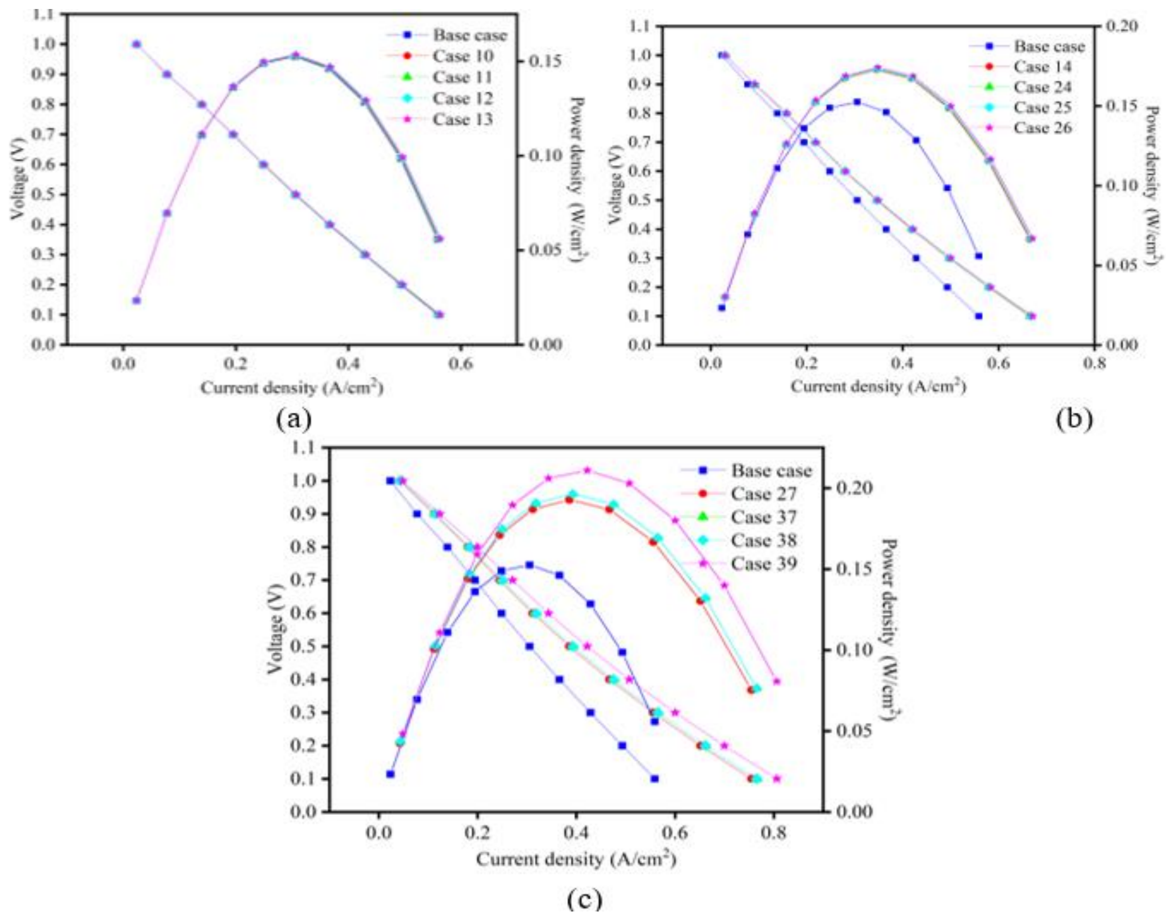

Figure 9. Effect on cell performance for anode and cathode convergent designs at different a/b ratio: (a)channel depth, rib width, and channel width are 1.5 (mm), (b) channel depth, rib and channel depth are 1.0 (mm), and (c) 0.5 (mm) of channel depth, rib width, and channel width.

3.2.2. Divergent channel design

The similar procedure was applied to the divergent channel designs. Inthese designs, cases withrib width, channel width, and channel depths of 1.5 (mm), 1.0 (mm), and 0.5 (mm)were considered as baseline cases. Within this framework, while the channel and rib widths and depths at the anode and cathode gas inlets and rib depth, width, were maintained constant, different geometries were created by varying the ratio of the outlet channel depth to the inlet channel depth (a/b) between 0.2 and 1 (Figure 10).

Figure 11 shows the impact of a/b ratios for the **divergent anode flow channel** on cell performance for different flow geometries. It is shown that variations in the a/b ratio do not have an immense impact on performance when the rib width, channel depth, and channel width are 1.5 (mm) and 1.0 (mm)(Fig. 11a).In addition, the cell performance variation was determined when the channel depth, rib width, and channel width are reduced to 0.5 (mm). For this anode proposed change in geometry, cell performance decreases as the a/b ratio reduces (Figs. 11b and 11c).

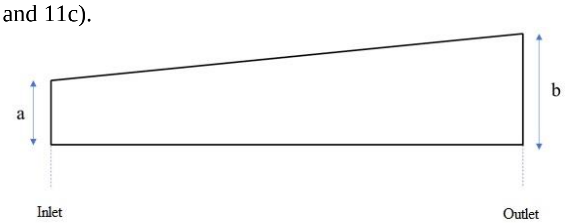

Figure 10. Divergent channel design

The effect of a/b ratios in the **divergent cathode flow** channel on cell performance for different flow geometries is given in Figure 12. It is seen that variations in the a/b ratio have no effect on the cell performance in which the rib width, channel depth, and channel width of 1.5 (mm), 1.0(mm), and 0.5 (mm). However, when compared to the base case, the test cases shown in Figures 12b and 12c demonstrate a significant increase in cell performance.

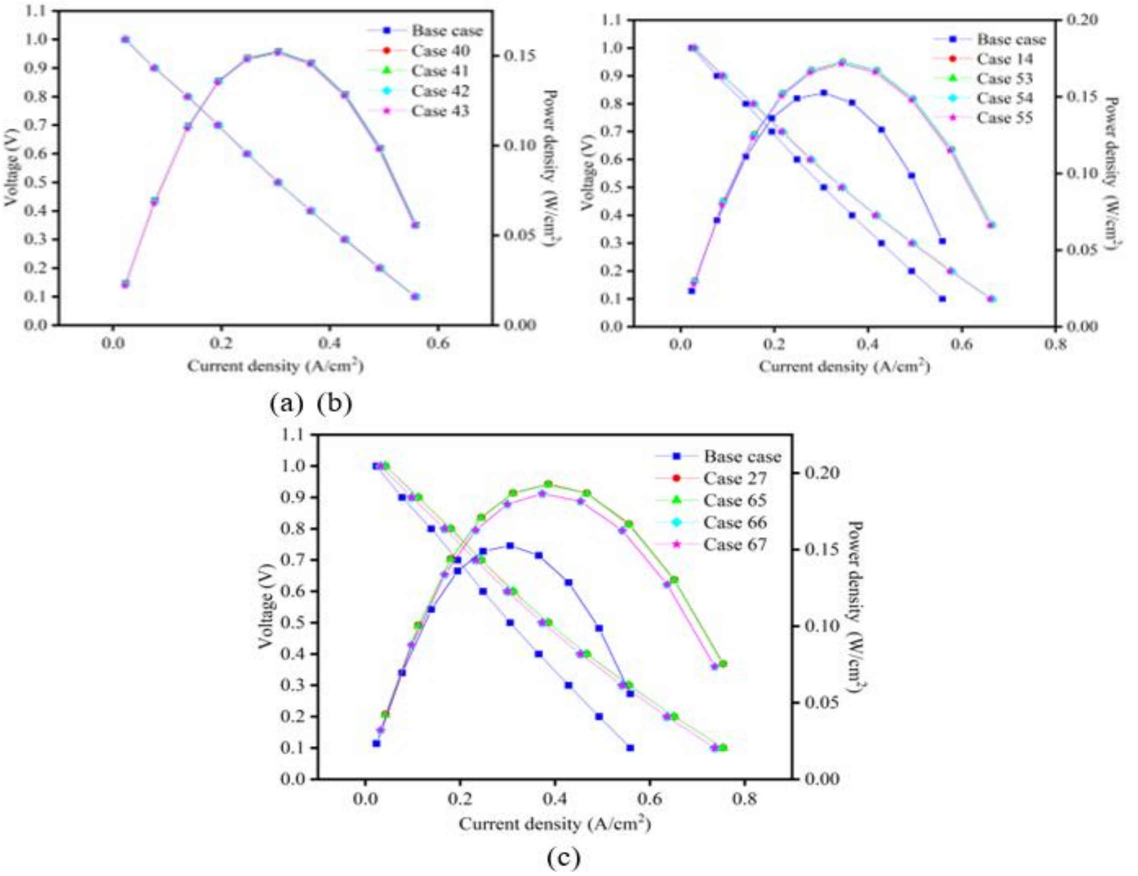

Figure 11. Divergent anode geometry impact on cell performance for different a/b ratio when channel depth, rib width, and channel width are 1.5 (mm) (a), 1.0 (mm) (b), and 0.5 (mm) (c)

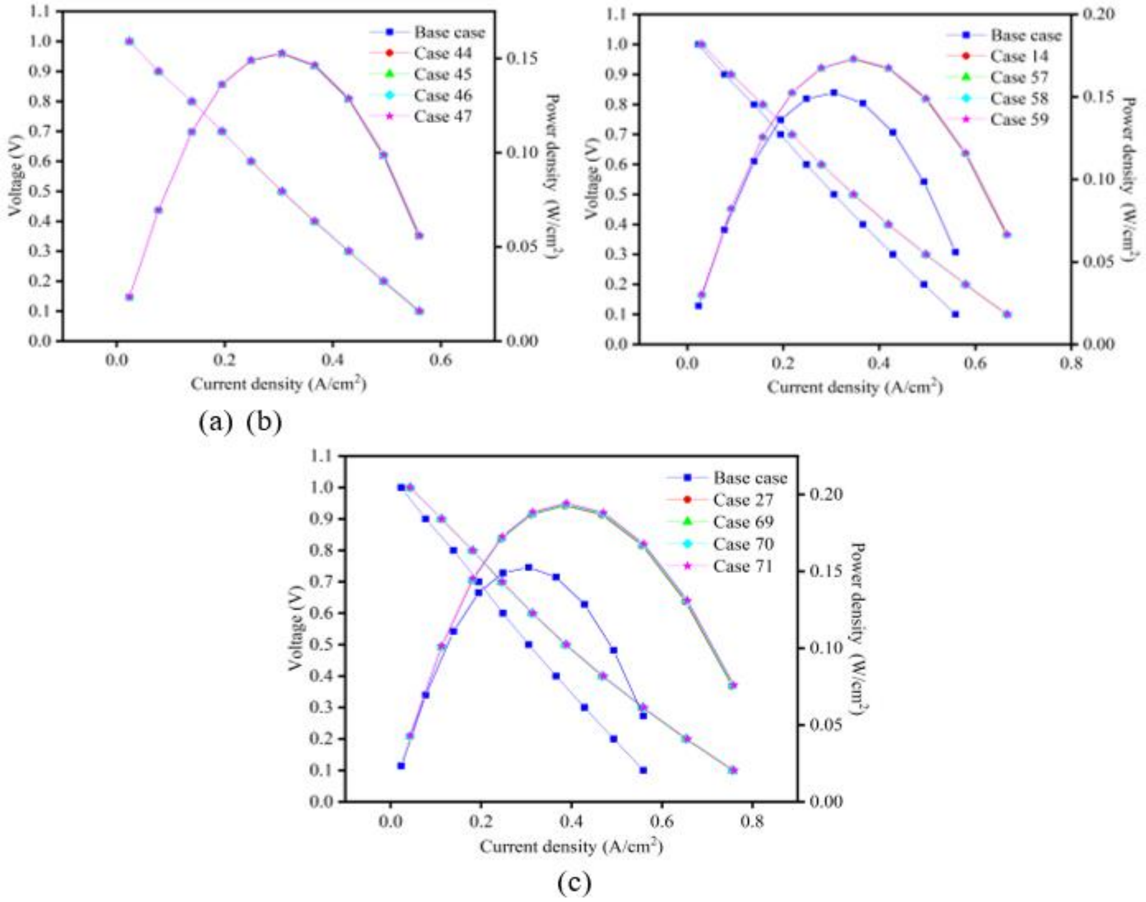

Figure 12. Divergent cathode geometry's impact on cell performance for different a/b ratio when

Figure 13 shows how flow field designs with the same a/b ratio on cell performance for **both anode and cathode flow** channels. It is seen that changes in the a/b ratio do not have significant effect on performance when the rib width, channel depth, and channel width are designed as 1.5 (mm) and 1.0(mm)(13a and 13b). For rib width, channel depth, and channel width 0.5 (mm), the cell performance decreases with decreasing a/b ratio. In addition, the test case shown in Figure 13b exhibit an improvement in the cell performance compared to the base case.

Case 39 revealed as the best configuration across the tested geometries, demonstrating the best electrochemical performance among the scenarios examined. This convergent channel design, especially at lower geometric dimensions (0.5 mm channel depth, rib width, and channel width), improved reactant distribution and mass transport characteristics in both the anode and cathode regions.

The maximum power density was 0.211 W/cm², up from 0.153 W/cm² for the baseline rectangular form. This is a 37.91% improvement. The greater performance of case example 39 demonstrates the effectiveness of convergent flow channel geometries in generating more uniform current density distribution and improved electrochemical activity, demonstrating such designs' potential for increasing SOFC efficiency.

Figure 14 depicts the distribution of the mass fractions of oxygen, hydrogen, and water produced by the SOFC. The mass fraction of oxygen at the inlet is 0.21; however, when it interacts with hydrogen along the electrolyte and membrane, its mass fraction at the outlet declines significantly, shown by the contour distribution in the cathode channel and at the electrolyte interface. Hydrogen flows in the opposite direction within the anode, with an inlet mass fraction of about 0.9. As it reacts with oxygen, its mass fraction in the anode channel gradually decreases to around 0.45. The electrochemical process produces water as a byproduct. Its mass fraction distribution is graphically illustrated, ranging from around 0.1 in the oxygen region to about 0.5 in the channel where water is dispersed as a result of the processes within the SOFC components.

Overall, the use of hydrogen for energy production in highly intensive industries is gaining attention, and fuel cell technologies can convert hydrogen and other gases into electricity and heat more efficiently compared to traditional Rankin and Brayton cycle technologies. In this article, the role of novel flow distribution in convergent and divergent geometrical designs was investigated and analyzed through both experimental and numerical approaches. The analysis presented in this research broadens the overall understanding of phenomena occurring in SOFCs and how tools such as COMSOL Multiphysics, which integrate multiple physics processes, can be used for developing novel technologies and enhance the efficiency of existing technologies.

The base case model represents the actual performance of a rectangular SOFC stack, while the evaluated scenarios provide a deeper insight into performance improvements achieved through different combinations of air and hydrogen channel flow geometries, particularly via convergent and divergent configurations. As shown in the literature review, rectangular channel designs exhibit better performance compared to triangular and trapezoidal geometries. Compared to similar studies analyzing the flow distribution in SOFC, this work contributes specifically to rectangular designs by incorporating convergent and divergent channels modifications, which have not beenextensively exploredin previous research.

Geometrical modifications can significantly enhance overall cell performance compared to base case, while also improving internal energy and mass transfer processes within SOFC. The findings and methodology presented in this study can be utilized by industry, academia, and relevant stakeholders interested in advancing technologies for energy system transformation.

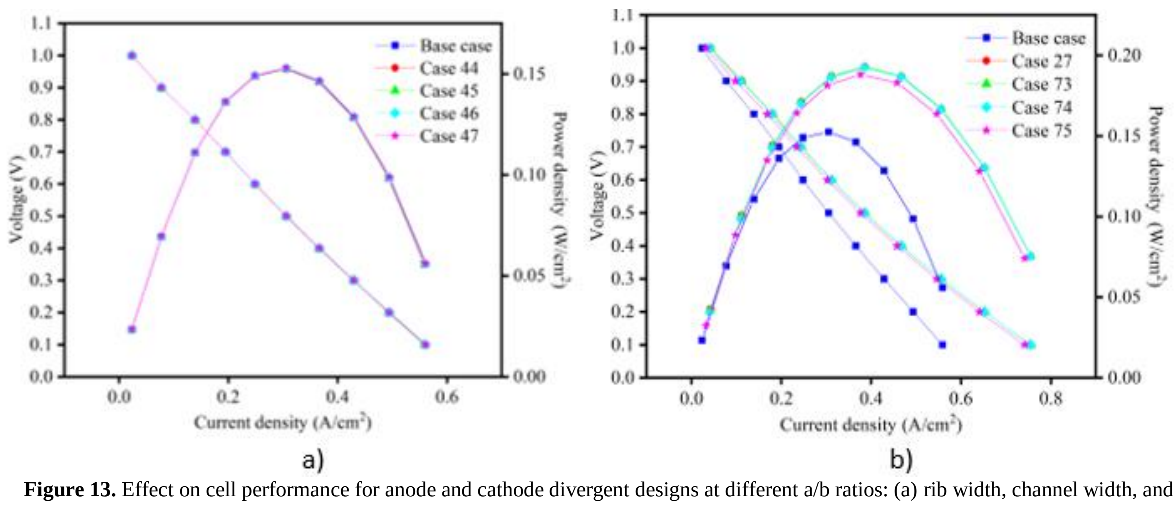

Figure 13. Effect on cell performance for anode and cathode divergent designs at different a/b ratios: (a) rib width, channel width, and channel depth 1.5 (mm), and (b) 0.5 (mm) of rib width, channel depth, and channel width.

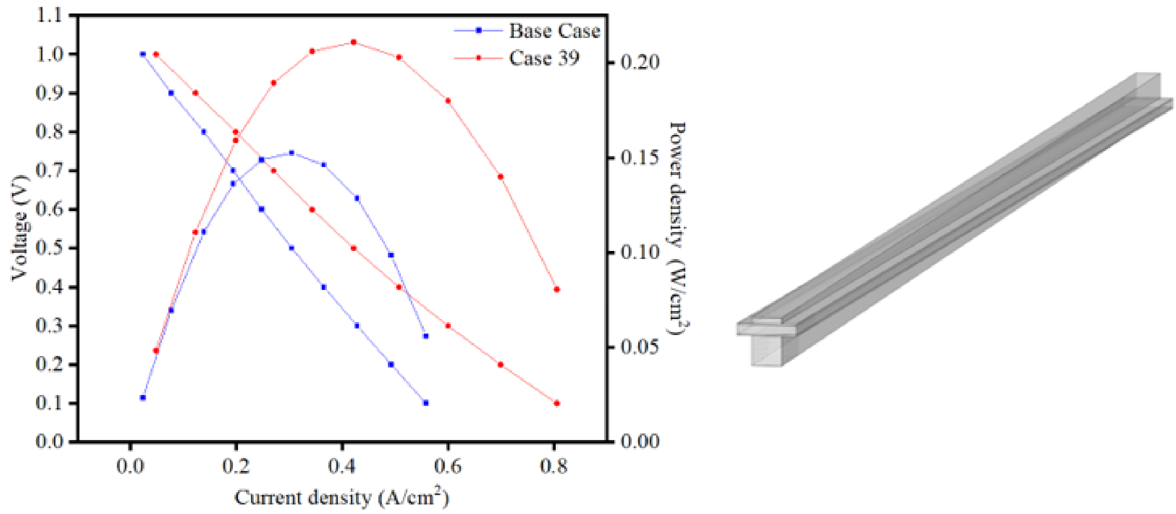

Figure 14. Cell performance analysis diagram of the best case (case 39) vs base case configuration

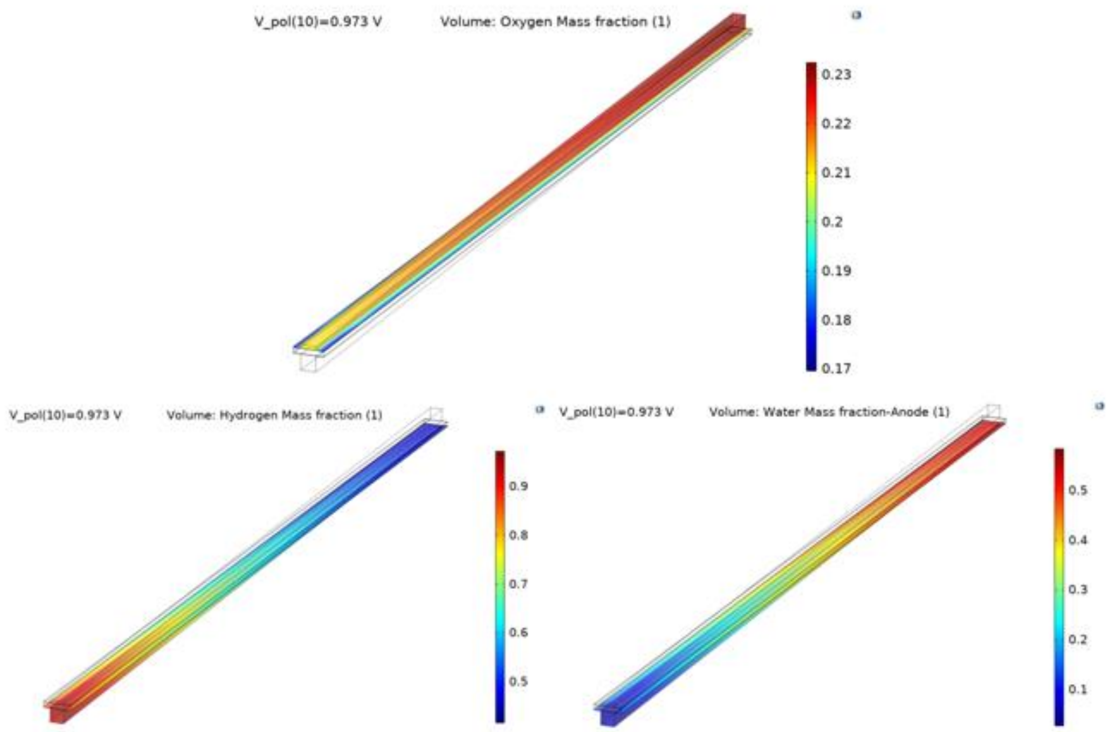

Figure 15. Mass distribution fraction for the assessed case 39.

4. CONCLUSION

The research aims to evaluate and develop experimental and numerical approaches for improving the performance of SOFC technologies that use hydrogen to produce power and heat. Experiments were conducted at Niğde Ömer Halisdemir University employing a reference SOFC case with a rectangular flow channel geometry on both cathode and anode sides. In addition, a numerical model was created and deployed in COMSOL Multiphysics for validation and performance improvement investigations. The rectangular channel reference (base) case, as well as other newly developed convergent and divergent flow distribution designs, were studied by applying a scenario-based methodology.

The analysis included 75 different anode and cathode channel counter-flow geometric novel designs (as shown in tables 3 and 4), through increasing (divergent) and decreasing (convergent) flow channel geometries in a counter-flow SOFC model. It has been determined that convergent and divergent channel designs do not significantly impact the performance of cells, especially in cases where channel depth, rib width, and channel width are 1.5 mm and 1 mm. An increase in performance is observed to others convergent and divergent channel designs, especially in cases where channel depth, rib width, and channel width are 0.5 mm.

The test cases that showed performance improvements are listed below: 14; 15-18; 20-22; 24-26; 27; 28-31; 32-35; 37-39; 53-55; 57-59; 65-67; 69-71; and 73-75. In contrast, the other test cases, which have been excluded from the total set of 75 simulations, showed no significant change in cell performance. Overall, this suggests that only certain geometric configurations have a substantial impact on SOFC performance, while the bulk of the evaluated changes have no effect under the conditions analyzed. Among the convergent designs, test case 39 yielded the highest cell performance with a maximum power density of 0.211 W/cm^2, while this value was found to be 0.153 W/cm^2 for the rectangular base case. This shows an improvement of 37.91% in the overall performance of SOFC due to proposed changes in the design of geometries.

Overall, the findings show that geometric modifications can significantly enhance SOFC performance and provide a strong basis for the future advancement of hydrogen-based energy systems. The findings may assist researchers and practitioners develop SOFC technologies in support to the shift to sustainable energy. Future research might look towards various materials and geometric configurations to obtain even better performance.

Acknowledgment

We express the deepest appreciation for the team from Niğde Ömer Halisdemir University who has been following this work and have contributed to the experiment and numerical modeling processes. The experimental studies have been conducted in Niğde Ömer Halisdemir University, respectively, in the Clean Energy Research Center, Prof. Dr. T. Nejat VezirogluIn Turkey, while numerical modeling were performed in the University of Prishtina in Kosovo.

Nomenclature

SOFC	Solid oxide fuel cell
H_2	hydrogen
CO_2	carbon dioxide
NO_x	nitrogen oxide
SO_x	sulfur oxide
SCCM	standard cubic centimeter per minute
YSZ	yttrium stabilized zirconia
MEG	membrane electrolyte group
T	temperature [K]
pa	absolute pressure [Pa]
L	length [m]
ε_p	porosity
k	permeability
i_a	current density at the anode [A/m^2]
i_c	current density at the cathode [A/m^2]
i_{0a}	exchange current density at the anode [A/m^2]
$i_{0,c}$	exchange current density at the cathode [A/m^2]
n	number of electrons
α_a	anodic charge transfer coefficient
α_c	cathode charge transfer coefficient
η	overvoltage [V]
u	velocity[m/s]
C_{h2}	molar concentration of hydrogen[mol/m^3]
$C_{h2, ref}$	reference concentration of hydrogen[mol/m^3]
C_{h2o}	molar concentration of water [mol/m^3]
$C_{h2o, ref}$	reference concentration of water [mol/m^3]
C_O	molar concentration ratio of oxidized species
C_{o2}	molar concentration of oxygen [mol/m^3]
$C_{o2, ref}$	reference concentration of oxygen[mol/m^3]
C_R	molar concentration ratio of reduced species
D_i	coefficient of diffusion[m^2/s]
D_i^T	thermal coefficient of diffusion [kg/ms]
E_{ct}	potential of electrode [V]
E_{eq}	difference potential equilibrium[V]
$E_{eq,a}$	anode equilibrium potential [V]
$E_{eq,c}$	cathode equilibrium potential[V]
F	constant of Faraday [C]
F_v	force volume [N/m^3]
R	universal gas constant [J/molK]
V_{cell}	voltage of cell [V]
V_{pol}	potential polarization [V]
x_k	fraction of a mole
φ_ℓ	electrolyte potential [V]
φ_s	electric potential [V]
ωi	mass fraction
ρ	mixture density[kg/m^3]
μ	dynamic viscosity [Pas]
ζ	permeability [m^2]
β	factor of correction

REFERENCES

[1] F. Zink, Y. Lu, and L. Schaefer, “A solid oxide fuel cell system for buildings,” *Energy Convers. Manag.*, vol. 48, no. 3, pp. 809–818, Mar. 2007, doi: 10.1016/j.enconman.2006.09.010.

[2] K. P. Recknagle, R. E. Williford, L. A. Chick, D. R. Rector, and M. A. Khaleel, “Three-dimensional thermo-fluid electrochemical modeling of planar SOFC stacks,” *J. Power Sources*, vol. 113, no. 1, pp. 109–114, Jan. 2003, doi: 10.1016/S0378-7753(02)00487-1.

[3] Z. Xu, X. Zhang, G. Li, G. Xiao, and J.-Q. Wang, “Comparative performance investigation of different gas flow configurations for a planar solid oxide electrolyzer cell,” *Int. J. Hydrog. Energy*, vol. 42, no. 16, pp. 10785–10801, Apr. 2017, doi: 10.1016/j.ijhydene.2017.02.097.

[4] S. Kapadia, W. K. Anderson, and C. Burdyshaw, “Channel shape optimization of solid oxide fuel cells using advanced numerical techniques,” *Implicit Solut. Navier–Stokes Equ. Spec. Issue Dedic. Drs WR Briley H McDonald*, vol. 41, no. 1, pp. 41–50, Feb. 2011, doi: 10.1016/j.compfluid.2010.09.021.

[5] I. Khazaee and A. Rava, “Numerical simulation of the performance of solid oxide fuel cell with different flow channel geometries,” *Energy*, vol. 119, pp. 235–244, Jan. 2017, doi: 10.1016/j.energy.2016.12.074.

[6] S. Akhtar, K. Chang, S. Siddiqa, M. Alam, and S.-W. Lee, “Impact of flow channel design optimization on the performance of solid oxide electrolysis cell (SOEC),” *Energy Rep.*, vol. 14, pp. 2686–2698, Dec. 2025, doi: 10.1016/ j.egyr.2025.09.011.

[7] Y. Tu, H. Lin, M. Chen, Z. Zhang, W. Cai, and Z. Zhu, “Design and numerical analysis of a Y-shaped flow channel for enhanced hydrogen production in solid oxide electrolysis cells,” *Int. J. Electrochem. Sci.*, vol. 19, no. 11, p. 100806, Nov. 2024, doi: 10.1016/j.ijoes.2024.100806.

[8] K. Mehmood, A. H. Khoja, N. Ahmed, Q. S. Ali, and H. Abdul Taha, “Numerical evaluation of flow field redesign in solid oxide electrolysis cells: Impact of converging flow channel structures on thermal uniformity and flow distribution through parametric analysis,” *J. Power Sources*, vol. 672, p. 239627, Apr. 2026, doi: 10.1016/j.jpowsour.2026.239627.

[9] K. Lee, S. Kang, and K.-Y. Ahn, “Development of a highly efficient solid oxide fuel cell system,” *Appl. Energy*, vol. 205, pp. 822–833, Nov. 2017, doi: 10.1016/j.apenergy.2017.08.070.

[10] T. Wu, G. Fan, Y. Wu, Y. Wang, and X. Xu, “Layout design optimization of the solid oxide fuel cell cogeneration system based on heat transfer and thermodynamics analysis,” *Appl. Therm. Eng.*, vol. 287, p. 129499, Feb. 2026, doi: 10.1016/j.applthermaleng.2025.129499.

[11] S. Wei *et al.*, “Optimizing fuel transport and distribution in gradient channel anode of solid oxide fuel cell,” *Chem. Eng. Sci.*, vol. 285, p. 119558, Mar. 2024, doi: 10.1016/j.ces.2023.119558.

[12] G. Li *et al.*, “Numerical and experimental study of effects of different flow channel structures on the performance of solid oxide fuel cell,” *J. Power Sources*, vol. 652, p. 237401, Oct. 2025, doi: 10.1016/j.jpowsour.2025.237401.

[13] C. Gong, X. Luo, Z. Tu, and S. H. Chan, “A novel flow channel design to achieve high temperature homogenization in solid oxide fuel cell,” *Int. J. Hydrog. Energy*, vol. 52, pp. 442–453, Jan. 2024, doi: 10.1016/j.ijhydene.2023.09.314.

[14] J. Wu, J. Hu, Z. Tu, and R. Hu, “A novel flow field design for the thermal management in planar solid oxide fuel cell,” *Int. J. Hydrog. Energy*, vol. 135, pp. 339–350, Jun. 2025, doi: 10.1016/j.ijhydene.2025.04.463.

[15] R. Gadhewal, V. S. Patnaikuni, and V. V. Ananthula, “Computational study on effect of geometric shape of flow channel and oscillatory gas supply on hot spot mitigation in PEM fuel cell with a 3D model of reconstructed gas diffusion layer,” *Int. Commun. Heat Mass Transf.*, vol. 171, p. 110155, Feb. 2026, doi: 10.1016/j.icheatmasstransfer.2025.110155.

[16] Z. Zeng *et al.*, “Effect of radial flows in fuel channels on thermal performance of counterflow tubular solid oxide fuel cells,” *Appl. Therm. Eng.*, vol. 219, p. 119577, Jan. 2023, doi: 10.1016/j.applthermaleng.2022.119577.

[17] C. Gong, S. Cai, W. Gang, Y. Guan, C. Wen, and Z. Tu, “Geometry and flow field optimization design of solid oxide fuel cell stack for temperature and flow rate uniformity improvement,” *Int. J. Hydrog. Energy*, vol. 160, p. 150625, Aug. 2025, doi: 10.1016/j.ijhydene.2025.150625.

[18] Y. Liu *et al.*, “Effects of bipolar plate flow channel configuration on thermal-electric performance of direct ammonia solid oxide fuel cell: Part I - Numerical study of channel section geometry,” *Int. J. Hydrog. Energy*, vol. 50, pp. 765–785, Jan. 2024, doi: 10.1016/j.ijhydene.2023.09.028.

[19] Y.-F. Li, S.-D. Sun, J.-L. Pang, Y. Dai, H.-Y. Zhang, and C.-X. Li, “Anode-side flow channel structure design for metal-supported solid oxide fuel cell: An investigation of discrete interconnect based on multi-physics coupling simulation,” *J. Power Sources*, vol. 653, p. 237705, Oct. 2025, doi: 10.1016/j.jpowsour.2025.237705.

[20] Y. Mehdizadeh Chellehbari, K. Adavi, J. Sayyad Amin, and S. Zendehboudi, “A numerical simulation to effectively assess impacts of flow channels characteristics on solid oxide fuel cell performance,” *Energy Convers. Manag.*, vol. 244, p. 114280, Sep. 2021, doi: 10.1016/j.enconman.2021.114280.

[21] V. A. Danilov and M. O. Tade, “A CFD-based model of a planar SOFC for anode flow field design,” *Int. J. Hydrog. Energy*, vol. 34, no. 21, pp. 8998–9006, Nov. 2009, doi: 10.1016/j.ijhydene.2009.08.073.

[22] A. Raj, A. P. Sasmito, and T. Shamim, “Numerical investigation of the effect of operating parameters on a planar solid oxide fuel cell,” *Energy Convers. Manag.*, vol. 90, pp. 138–145, Jan. 2015, doi: 10.1016/j.enconman.2014.10.055.

[23] J. D. Duhn, A. D. Jensen, S. Wedel, and C. Wix, “Optimization of a new flow design for solid oxide cells using computational fluid dynamics modelling,” *J. Power Sources*, vol. 336, pp. 261–271, Dec. 2016, doi: 10.1016/j.jpowsour.2016.10.060.

[24] X. Li, W. Shi, and M. Han, “Optimization of interconnect flow channels width in a planar solid oxide fuel cell,” *Int. J. Hydrog. Energy*, vol. 43, no. 46, pp. 21524–21534, Nov. 2018, doi: 10.1016/j.ijhydene.2018.09.061.

[25] R. J. Boersma and N. M. Sammes, “Computational analysis of the gas-flow distribution in solid oxide fuel cell stacks,” *J. Power Sources*, vol. 63, no. 2, pp. 215–219, Dec. 1996, doi: 10.1016/S0378-7753(96)02476-7.

[26] A. Li, C. Song, and Z. Lin, “A multiphysics fully coupled modeling tool for the design and operation analysis of planar solid oxide fuel cell stacks,” *Appl. Energy*, vol. 190, pp. 1234–1244, Mar. 2017, doi: 10.1016/j.apenergy.2017.01.034.

[27] M. Ni, “2D thermal-fluid modeling and parametric analysis of a planar solid oxide fuel cell,” *Energy Convers. Manag.*, vol. 51, no. 4, pp. 714–721, Apr. 2010, doi: 10.1016/j.enconman.2009.10.028.

[28] R. J. Kee, P. Korada, K. Walters, and M. Pavol, “A generalized model of the flow distribution in channel networks of planar fuel cells,” *J. Power Sources*, vol. 109, no. 1, pp. 148–159, Jun. 2002, doi: 10.1016/S0378-7753(02)00090-3.

[29] Haleemah J. Mohammed, Dhuha R. Nayyaf, Karrar A. Hammoodi, Karrar K. Abdul Hussein, Ahmed Mohsin Alsayah, Saif Ali Kadhim. ‘Preparation and Evaluation of Nanomembranes for Proton Exchange Membrane Fuel Cells Modeling Using Artificial Neural Networks’ Jordan Journal of Mechanical and Industrial Engineering. vol. 18, pp. 705-709, Dec. 2024, https://doi.org/10.59038/jjmie/180406.

[30] R. T. Nishida, S. B. Beale, and J. G. Pharoah, “Comprehensive computational fluid dynamics model of solid oxide fuel cell stacks,” *Int. J. Hydrog. Energy*, vol. 41, no. 45, pp. 20592–20605, Dec. 2016, doi: 10.1016/j.ijhydene.2016.05.103.

[31] Y. Ma, Z. Shi, J. Hu, S. Shen, and S. Wang, “Experimental study on the current distribution in planar solid oxide fuel cells by a novel segmentation method,” *J. Power Sources*, vol. 655, p. 237876, Nov. 2025, doi: 10.1016/j.jpowsour.2025.237876.

[32] F. Huang, X. Li, B. Wang, and T. Li, “Experimental and numerical study of a multi-channel solid oxide fuel cell stack: performance enhancement and compact design,” *J. Power Sources*, vol. 669, p. 239397, Mar. 2026, doi: 10.1016/j.jpowsour.2026.239397.

[33] L. F. G. Setz, I. Santacruz, M. T. Colomer, S. R. H. Mello-Castanho, and R. Moreno, “Fabrication of Sr- and Co-doped lanthanum chromite interconnectors for SOFC,” *Mater. Res. Bull.*, vol. 46, no. 7, pp. 983–986, Jul. 2011, doi: 10.1016/j.materresbull.2011.03.019.

[34] P. Duran, J. Tartaj, F. Capel, and C. Moure, “Formation, sintering and thermal expansion behaviour of Sr- and Mg-doped $LaCrO_3$ as SOFC interconnector prepared by the ethylene glycol polymerized complex solution synthesis method,” *J. Eur. Ceram. Soc.*, vol. 24, no. 9, pp. 2619–2629, Aug. 2004, doi: 10.1016/j.jeurceramsoc.2003.09.016.

[35] B. Timurkutluk, S. Toros, S. Onbilgin, and H. G. Korkmaz, “Determination of formability characteristics of Crofer 22 APU sheets as interconnector for solid oxide fuel cells,” *Int. J. Hydrog. Energy*, vol. 43, no. 31, pp. 14638–14647, Aug. 2018, doi: 10.1016/j.ijhydene.2018.04.243.

[36] B. Timurkutluk and S. Onbilgin, “Design and fabrication of novel interconnectors for solid oxide fuel cells via rubber pad forming,” *Int. J. Energy Res.*, vol. 44, no. 11, pp. 8716–8729, Sep. 2020, doi: 10.1002/er.5565.